Eur. Phys. J. Special Topics **167**, 33–39 (2009)
© EDP Sciences, Springer-Verlag 2009
DOI: 10.1140/epjst/e2009-00933-8

THE EUROPEAN PHYSICAL JOURNAL SPECIAL TOPICS

Regular Article

Atomic-scale X-ray structural analysis of self-assembled monolayers on Silicon

J.-C. Lin[1], J.A. Kellar[1], J.-H. Kim[2], N.L. Yoder[1], K.H. Bevan[3], S.T. Nguyen[2], M.C. Hersam[1,2], and M.J. Bedzyk[1,a]

[1] Northwestern University, Materials Science and Engineering, Evanston, IL 60208, USA
[2] Northwestern University, Chemistry, Evanston, IL 60208, USA
[3] Purdue University, Electrical and Computer Engineering, West Lafayette, IN 47907, USA

Abstract. Two related self-assembled monolayers (SAMs), 4-bromostyrene (BrSty) and 4-bromophenylacetylene (BPA), are photochemically grown from solution on to the monohydride-terminated Si(111) surface. The atomic-scale structures of the resulting SAMs are examined by X-ray standing waves (XSW), X-ray reflectivity (XRR), X-ray fluorescence, atomic-force microscopy (AFM), X-ray photoelectron spectroscopy (XPS), and density functional theory (DFT). The coverage is 0.5 ML. The results show that in each case the molecule covalently bonds to a single Si T_1 site and stands up-right with a slight molecular tilt of 17° that leaves the Br terminal end over a neighboring T_4 site. The Br height is 8.5 Å (BrSty) and 8.6 Å (BPA) above the top surface Si atom. The combined XSW and XRR results rule-out two alternative bonding models predicted by DFT that have the root of the molecule bonded to two neighboring top Si surface atoms. Based on the XSW 111 and 333 coherent fractions, the BPA/Si(111) has a reduced vertical Br distribution width in comparison to BrSty. This greater rigidity in the molecular structure is correlated to a C=C bond at the root.

1 Introduction

Silicon surfaces functionalized with covalently bonded organic molecules are of interest for applications in electronic devices and medical sensors [1–5]. For utilization of this type of self-assembled monolayer (SAM) in real devices, the structural details, such as bonding configuration, molecular orientation, and molecular packing within the film are critical [4,5].

Complementary to the top-down topographical imaging of scanning probe microscopy (SPM), *in situ* hard X-ray probes are able to penetrate and quantitatively study the in-depth intrinsic structure of SAMs on an atomic length-scale [6,7]. By combining X-ray scattering and X-ray spectroscopy, it is possible to make this structural information element-specific. The X-ray standing wave (XSW) method [8–11], which combines X-ray diffraction with X-ray fluorescence (XRF), is used to circumvent the "phase-problem" and directly measure the *hkl* complex Fourier components of an individual XRF-selected sublattice.

XSW has been widely used for determining the precise lattice location of adatoms on single crystal surfaces [9–12]. Herein, we show an atomic-scale SAM analysis method that combines XSW with X-ray reflectivity (XRR), X-ray photoelectron spectroscopy (XPS), atomic-force microscopy (AFM) and density functional theory (DFT). We apply this to the study of 4-bromophenylacetylene (BPA) SAM on a Si(111) surface. The BPA result is directly compared with our previously published result for 4-bromostyrene (BrSty) [13], since these two molecules

[a] e-mail: bedzyk@northwestern.edu

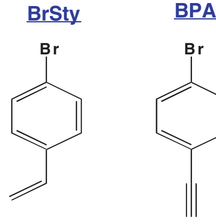

Fig. 1. Chemical schematic of the two molecules used in the study.

(shown in Fig. 1) are identical with the exception of their respective terminal group (a C=C bond for BrSty and a C≡C bond for the BPA molecule before the hydrosilylation step). The terminal Br, which serves as an XRF marker-atom, also enables further functionalization of the SAM. These two molecules were chosen because the delocalized electrons in their aromatic rings make them of interest for electronic applications. After hydrosilylation, the C≡C bond in BPA converts to a C=C bond and the C=C bond in BrSty becomes a C–C bond. A direct structural comparison will show the feasibility of engineering SAMs with different bonding configurations.

2 Experimental

A monohydride-terminated Si(111) surface was prepared using a modified procedure from Higashi et al. [13,14]. For the photochemical reaction, a *254 nm* UV pen lamp was used and the entire process was performed in a slightly positive N_2 pressure glove box. The pen lamp was positioned about 1 cm above the substrate to trigger the reaction. A 2 *h* UV exposure time was used for BrSty [13], while 20 *h* was used for BPA in order to achieve the identical coverage (*∼0.5 ML*) as determined by XRF. Later, samples were brought out of the glove box and sonicated with anhydrous methylene chloride and chloroform until sharp step edges were recovered under AFM. The preservation of the silicon atomic terrace before and after the film growth confirms the accomplishment of atomically flat surfaces. In-house XPS was used to verify the Br–C bonding, which legitimated the use of Br as the marker for structural characterization. XPS also confirmed that no oxidation of the silicon substrate had occurred. A more detailed discussion of the above sample preparation, AFM and XPS can be found elsewhere [13,15,16].

In order to determine the SAM thickness and interface roughness, specular reflectivity measurements were carried out in-house at NU's X-ray Diffraction Facility. The XRR analysis uses a 1*D* molecule structure factor based on the z coordinates of the non-hydrogen atoms. Samples were sealed within a dry-nitrogen-flow cell during X-ray exposure (also true for the synchrotron XSW measurements) to minimize damage to the SAM.

The SAM/Si(111) XSW analysis, which is described in more detail elsewhere [13], was performed at the Advanced Photon Source (APS) 5ID-C undulator station [17]. The incident photon energy was tuned to be above the Br K-edge in order to excite Br Kα fluorescence. The incident beam was attenuated during sample alignment and a fast shutter was used to minimize integrated dose. The footprint of the beam on the sample was moved to a fresh unradiated spot before any significant damage occurred. In the XSW measurement the reflectivity and XRF spectra are simultaneously collected while scanning through an H = *hkl* Bragg reflection [9,11]. The normalized Br fluorescence yield is given by

$$Y(\theta) = 1 + R(\theta) + 2\sqrt{R(\theta)} f_H \cos[v(\theta) - 2\pi P_H] \tag{1}$$

where the reflectivity (R) and XSW phase (v) are derived from dynamical diffraction theory. The analysis produces a directly measured *hkl* Fourier amplitude, f_H, and phase, P_H, for the Br atomic distribution. The summation of these Fourier components over a measured volume of reciprocal space leads to a model-independent 3*D* direct space Br atomic map [9,12,18,19]:

$$\rho(\boldsymbol{r}) = \sum_{H} f_H \exp[2\pi i(P_H - \boldsymbol{H}\cdot\boldsymbol{r})] = 1 + 2\sum_{\substack{H\neq -H\\ H\neq 0}} f_H \cos[2\pi(P_H - \boldsymbol{H}\cdot\boldsymbol{r})]. \tag{2}$$

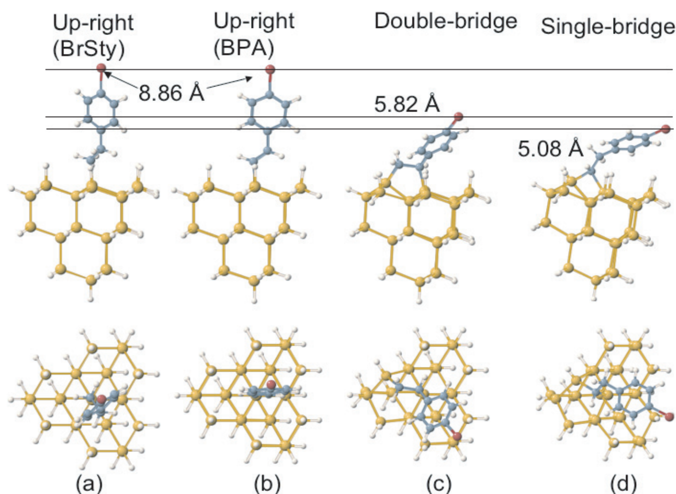

Fig. 2. (Colour online) Possible bonding configurations of BrSty and BPA molecules from cluster DFT calculations. (a) and (b) "Up-right" structures of BrSty and BPA SAMs. (c) Double-bridge structure. (d) Single-bridge structure. The listed Br heights are relative to the topmost Si.

A side-by-side comparison of the Br Kα yield from the SAM to the As Kβ yield from an arsenic implanted standard determines the Br coverage. For Si(111), 1 *monolayer (ML)* coverage corresponds to *7.83 atoms/nm*^{2}.

3 Results and discussion

The possible bonding configurations predicted by cluster DFT calculations of both BrSty and BPA SAMs are shown in Fig. 2. The clusters were first constructed using HyperChem Release 7 and optimized using molecular mechanics. The clusters were further optimized using DFT within the Q-Chem electronic structure package [20]. For both SAMs, each single molecule can attach to one surface silicon and form an "up-right" structure (Fig. 2(a) & 2(b)), or BPA can react with two surface silicon atoms to form either a "double-bridge" (Fig. 2(c)) or "single-bridge" (Fig. 2(d)) structure. Although the last two models suffer from a lattice distortion due to the limited size of silicon cluster used, it is still obvious that the bridge-like structures predict lower Br heights. The direct comparison of (1×1) to (2×1) models in our periodic DFT study (a unit of eight layers slabs used in SIESTA [21]) shows that the molecular packing density can affect the Br height by as much as 2.4 Å. This discrepancy is smaller than the discrepancy caused by the different bonding configurations and suggests that the Br height can be used for probing the bonding configuration.

Since specular reflectivity only senses the $1D$ electron density profile [22], for which the models in Fig. 2(a)–(b) are essentially identical, the four models reduce to three distinguishable XRR simulations, which are shown in Fig. 3 together with the BrSty and BPA XRR data. The A1 ("up-right"), A2 ("double-bridge") and A3 ("single-bridge") XRR simulation curves use the same structure parameters: packing density $\Theta = 0.5\,ML$, roughness $\sigma = 2.0$ Å for the static Gaussian vertical displacement distribution for all atoms in the molecule and $\beta = 0.5$ for the interface roughness parameter [23].

As expected, the Q value of the anti-reflection dip is highly sensitive to the film thickness. In Fig. 3, the "up-right" model (A1, $thickness = 8.9$ Å) better fits both BrSty and BPA data than the two bridge models. After considering the possible tilting of the molecules and the roughness of the films, the best fit for the thickness of the BrSty SAM is *8.5* Å and *8.7* Å for the BPA SAM. This result supports the chain reaction growth mechanism proposed by Chidsey [24]. If the formation of bridge-like structures dominated the film growth, the reaction of the molecules

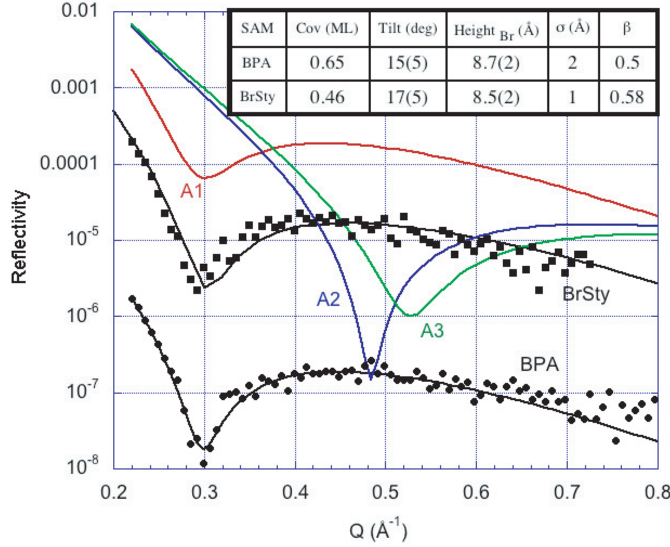

Fig. 3. Specular XRR data of BrSty (filled squares) and BPA (filled circles) SAMs are plotted together with simulations based on models from Figure 2. A1 corresponds to the "up-right" model (2(a) & 2(b)), A2 corresponds to the "double-bridge" model (2(c)) and A3 represents the "single-bridge" model (2(d)). For purposes of clarity, the vertical offsets are $\times 10^2$ for BrSty and $\times 10^3$ for A1, A2 and A3. The inset table lists the structural parameters from the best fits. Tilt angle $\theta = \mathrm{Cos}^{-1}(\mathrm{H_{Br}}/\mathrm{L_{mol}})$ where $\mathrm{H_{Br}}$ is the measured height of the Br atom and $\mathrm{L_{mol}}$ is the Si to Br length of the molecule from the DFT predictions. $\mathrm{L_{BPA}} = 9.0$ Å and $\mathrm{L_{BrSty}} = 8.9$ Å.

onto the surface would not have required the abstraction of any additional hydrogen from neighboring Si; therefore, there would be no chain reaction.

The (111) XSW results are shown in Fig. 4 and all the specular and off-specular XSW f_H and P_H measured values are listed in Table 1.

Table 1. XSW measured values for Br coherent fractions (f_H) and coherent positions (P_H). The chosen origin is at a bulk-like Si position in the top of the bi-layer.

(hkl)	(111)		(333)		$(11\bar{1})$		(220)	
	Coh. f	Coh. P	Coh. f	Coh. P	Coh. f	Coh. P	Coh. f	Coh. P
BrSty	0.35(2)	0.71($\underline{2}$4)	0.08(2)	0.10(6)	0.25(2)	0.35(2)	0.11(2)	1.00(3)
BPA	0.61(2)	0.74(2)	0.29(4)	0.32(4)	0.15(2)	0.29(2)	0.10(2)	0.92(3)

The $\rho(\boldsymbol{r})$ in Eq. (2) that the XSW method measures is the time-averaged (and domain-averaged) distribution of all Br in the mm^2 X-ray foot print as projected into a substrate Si unit cell. Qualitatively, f_H measures the spatial spread in the Br distribution relative to the standing wave period. The value of f_H is directly proportional to the non-random fraction C, which is the fraction of Br atoms at specific locations. A larger distribution spread relative to the d-spacing will result in a smaller f_H. Since the Si (111) and $(11\bar{1})$ reflections have the same lattice d-spacing, a comparison of their respective f_H values is a comparison of the vertical and lateral spread in the Br distribution after all domains have been projected into a single unit cell. In Table 1, both SAMs have f_{111} greater than $f_{11\bar{1}}$. The main contributing factors to this are: 1) domain averaging, in which the 3-fold symmetry related domains, all have Br at the same vertical height, but at three different lateral positions that exhibit 3-fold symmetry, and 2) the molecule that tethers Br to Si has a greater freedom to azimuthally rotate than to stretch. Interestingly, f_{111} is significantly higher for the BPA SAM than for the BrSty. Assuming that the up-right configuration is the only conformation for both BrSty and BPA SAMs, the

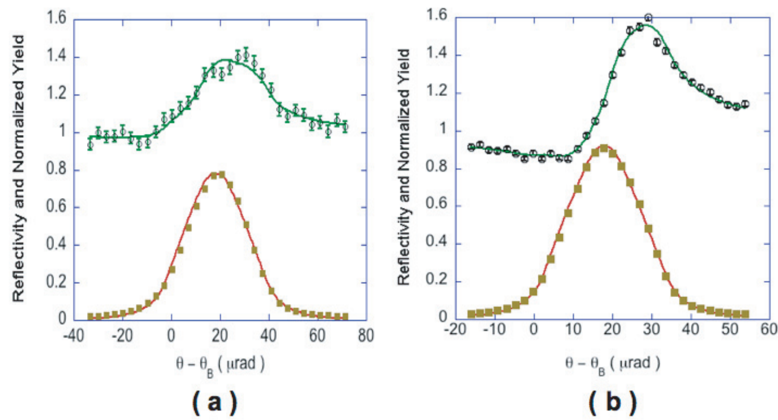

Fig. 4. The 111 XSW results of (a) BrSty and (b) BPA SAMs on Si(111). At the top of (a) and (b) are shown the Eq. (1) fits to the Br Kα fluorescence yield data. The fit determined parameters, f_{111} and P_{111}, are listed in Table 1. The 111 Si reflectivity data and theory fits are shown in the bottom of (a) and (b). All four of these dynamical diffraction theory derived curves are convoluted with the emission function from the upstream Si(111) 2-bounce channel-cut post-monochromator.

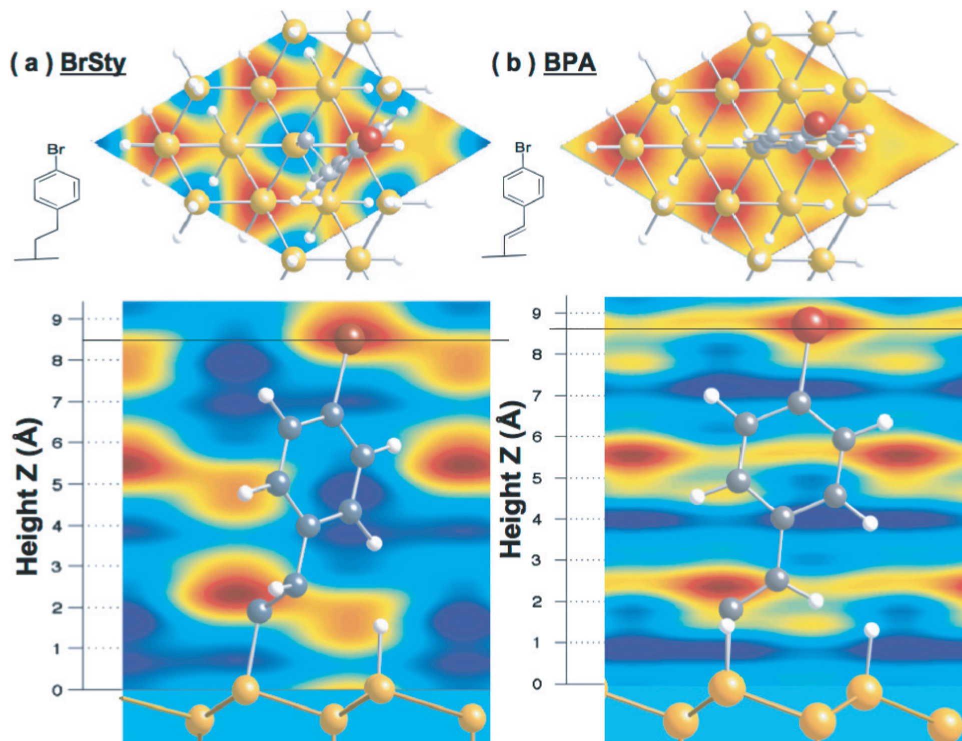

Fig. 5. (Colour online) Projected ball-and-stick models for (a) BrSty and (b) BPA SAMs on Si(111) superimposed on top of cuts through the XSW measured Br atomic maps from Eq. (2). The lower images are side-view cuts that coincide with the T_1, T_4 and H_3 high-symmetry sites of the Si(111) 1×1 surface. The upper images are top-view cuts parallel to the (111) surfaces at the measured Br heights indicated by the horizontal lines. The superimposed models of BrSty and BPA SAMs are based on cluster DFT predictions (Figs. 2(a) and 2(b)) with additional tilting to match the measured heights from XSW and XRR results.

vertical spread of Br can be analytically determined by the comparison of f_{111} with f_{333}. f_H can be expressed as the product of non-random fraction C, geometrical factor a_H and the Debye-Waller factor D_H. $D_H = \exp(-2\pi^2\sigma_H^2/d_H^2)$ treats the averaged displacement field of the Br atomic centers as a Gaussian distribution with width σ_H. Using the Table 1 f_{111} and f_{333} values, and assuming $a_{111} = a_{333} = 1$ (i.e., a single Br height), we compute that $C = 0.7$ and $\sigma_{111} = 0.22$ Å for the BPA SAM, whereas $C = 0.4$ and $\sigma_{111} = 0.30$ Å for the BrSty SAM. The greater non-random fraction and smaller distribution spread of Br in the BPA SAM suggests that this overall improvement to the vertical order can be accredited to the more rigid C=C bond at the bottom of BPA in contrast to the C-C bond for BrSty.

The directly measured $3D$ Br atomic density map, relative to the Si lattice, is produced by inserting the measured f_H and P_H values from Table 1 (and their 3-fold symmetry equivalents) into Eq. (2). $2D$ cuts of this Br atomic density map for the two different SAMs are shown in Fig. 5, together with our proposed structures based on cluster DFT calculations.

Because the Br density map is generated by a set of allowed *hkl* Si reflections, it has the same periodicity as the Si primitive (rhombohedral) unit cell. Since the hexagonal unit cell we chose in Fig. 5 is three times the size of the primitive unit cell, there will be three translational symmetry equivalent Br maxima in each map. Both SAMs have Br hot spots at: 1) ∼*8.6* Å high and laterally above the T_4 site, 2) ∼*5.5* Å high and laterally above the H_3 site, and 3) ∼*2.4* Å and laterally above T_1 site. From the XRR results, the films thicknesses were determined to be ∼*8.6* Å, which rules out the two lower hot spots. Using the coherent positions from Table 1, the Br heights of SAMs are determined to be $h = [2 + P_{111}]d_{111} = 8.5$ Å for BrSty and *8.6* Å for BPA. A comparison to the slightly higher DFT calculated heights shown in Figs. 2(a) and 2(b), would indicate that the molecules are tilted further inward than predicted by DFT. Using the DFT molecular lengths, there is a 17° latitudinal tilt for both molecules with the molecules leaning toward the Si T_4 site as shown in Fig. 5. Both XSW results for the Br heights agree with the XRR analysis within the error of the two measurements, namely ±0.05 Å for XSW and ±0.2 Å for XRR.

4 Summary

We have combined AFM, XPS, XRR, XSW and DFT techniques to determine the structures of wet photochemically prepared BrSty and BPA SAMs on H-Si(111). We find that both SAMs have a single covalent C-Si bond at the Si T_1 site and a 17° molecular tilt toward a neighboring T_4 site. With the stronger C = C bond than C–C at the root, the BPA SAM shows a greater rigidity in the molecular structure vertically than the BrSty SAM. Since the efficiency of molecular electronics is greatly affected by the order of its conformation [4,5], the utilization of a C=C bond can potentially improve device performance.

This work was supported by the Nanoscale Science and Engineering Initiative of the National Science Foundation (Award Numbers EEC-0118025 and ECS-0506802). The authors thank the DND-CAT staff and Jerrold Carsello of the NU X-ray Lab for technical assistance. Use of the APS at Argonne National Laboratory was supported by the DOE/BES under Contract No. DE-AC02-06CH11357. DND-CAT is supported in part by the State of Illinois. This work made use of NU Central Facilities supported by the MRSEC through NSF Contract No. DMR-0520513. Computational resources were provided by the National Science Foundation Network for Computational Nanotechnology.

References

1. P. Wagner, S. Nock, J.A. Spudich, W.D. Volkmuth, S. Chu, R.L. Cicero, C.P. Wade, M.R. Linford, C.E.D. Chidsey, J. Struct. Biol. **119**, 189 (1997)
2. A. Salomon, T. Böcking, J.J. Gooding, D. Cahen, Nano Lett. **6**, 2873 (2006)
3. T. Strother, W. Cai, X. Zhao, R.J. Hamers, L.M. Smith, J. Am. Chem. Soc. **122**, 1205 (2000)
4. C.D. Dimitrakopoulos, P.R.L. Malenfant, Adv. Mater. **14**, 99 (2002)

5. J. Cornil, D. Beljonne, J.-P. Calbert, J.-L. Bredas, Adv. Mater. **13**, 1053 (2001)
6. M. Mezger, H. Reichert, S. Schöder, J. Okasinski, H. Schröder, H. Dosch, D. Palms, J. Ralston, V. Honkimäki, Proc. Natl. Acad. Sci. **103**, 18401 (2006)
7. M.R. Linford, P. Fenter, P.M. Eisenberger, C.E.D. Chidsey, J. Am. Chem. Soc. **117**, 3145 (1995)
8. B.W. Batterman, Phys. Rev. A **133**, 759 (1964)
9. M.J. Bedzyk, L.W. Cheng, Rev. Mineral Geochem. **49**, 221 (2002)
10. J.A. Golovchenko, J.R. Patel, D.R. Kaplan, P.L. Cowan, M.J. Bedzyk, Phys. Rev. Lett. **49**, 560 (1982)
11. J. Zegenhagen, Surf. Sci. Rep. **18**, 199 (1993)
12. A.A. Escuadro, D.M. Goodner, J.S. Okasinski, M.J. Bedzyk, Phys. Rev. B **70**, 235416 (2004)
13. R. Basu, J.C. Lin, C.Y. Kim, M.J. Schmitz, N.L. Yoder, J.A. Kellar, M.J. Bedzyk, M.C. Hersam, Langmuir **23**, 1905 (2007)
14. G.S. Higashi, Y.J. Chabal, G. W. Trucks, K. Raghavachari, Appl. Phys. Lett. **56**, 656 (1990)
15. J.-H. Kim, J.-C. Lin, J.A. Kellar, M.C. Hersam, M.J. Bedzyk, S.T. Nguyen, Adv. Mater. (submitted)
16. J.A. Kellar, J.-C. Lin, J.-H. Kim, N.L. Yoder, K.H. Bevan, G.Y. Stokes, F. Geiger, S.T. Nguyen, M.J. Bedzyk, M.C. Hersam, J. Phys. Chem. C (2009) (in press)
17. D.A. Walko, O. Sakata, P.F. Lyman, T.-L. Lee, B.P. Tinkham, J.S. Okasinski, Z. Zhang, M.J. Bedzyk, AIP Conf. Proc. **705**, 1166 (2004)
18. L. Cheng, P. Fenter, M.J. Bedzyk, N.C. Sturchio, Phys. Rev. Lett. **90**, 255503 (2003)
19. J.S. Okasinski, C.-Y. Kim, D.A. Walko, M.J. Bedzyk, Phys. Rev. B **69**, 0414041 (2004)
20. J. Kong, C.A. White, A.I. Krylov, D. Sherrill, et al., J. Comput. Chem. **21**, 1532 (2000)
21. J.M. Soler, E. Artacho, J.D. Gale, A. Garcia, J. Junquera, P. Ordejon, D. Sanchez-Portal, J. Phys. Cond. Mat. **14**, 2745 (2002)
22. J. Als-Nielsen, D. McMorrow, *Elements of Modern X-Ray Physics* (John Wiley & Sons, Ltd., 2001)
23. I.K. Robinson, D.J. Tweet, Rep. Prog. Phys. **55**, 599 (1992)
24. R.L. Cicero, M.R. Linford, C.E.D. Chidsey, Langmuir **16**, 5688 (2000)